Single-Mode Vertical-Cavity Surface-Emitting Lasers Array With Zn-Diffusion Aperture for High-Power, Single-Spot, and Narrow Divergence Angle Performance

Jia-Liang Yen, Kai-Lun Chi, Jia-Wei Jiang, Ying-Jay Yang, and Jin-Wei Shi, *Senior Member, IEEE*

***Abstract*— A single-mode vertical-cavity surface-emitting laser (VCSEL) array at 850 nm with excellent performance in terms of high output power, single-lobe far-field, and narrow divergence angle has been demonstrated. By use of the Zn-diffusion process with proper sizes of oxide current-confined and Zn-diffusion optical apertures, each unit of VCSEL in the demonstrated array is highly single-mode (side-mode suppression ratio >30 dB) with a narrow far-field divergence angle (∼5°) and an extremely high maximum single-mode output power (∼7.1 mW). Due to the excellent single-mode performance of each VCSEL unit, the 10 × 10 array exhibits a single-lobe and nearly circular symmetric far-field pattern, very narrow divergence angle (∼4°), and output power as high as around 187.4 mW. Furthermore, its bias-dependent output optical spectra measured in different positions of array shows very high similarity. This result indicates that the excellent uniformity of single-mode performance of each VCSEL unit in the array. The far-field pattern simulation results indicate that although the coherence in our array is low, its output beam quality is as high as that of a single-mode unit VCSEL, which exhibits a near diffraction limited M square factor ($M^2 \approx 2$).**

***Index Terms*— Semiconductor lasers, vertical cavity surface emitting lasers.**

I. Introduction

THE requirement of high-power infrared light sources has tremendously increased due to its applications of infrared lighting and security monitoring in the darkness. Recently, a very high-power (1 Watt) and high-efficiency (∼70 %) light-emitting diode (LED) at infrared wavelength (850 nm) has been demonstrated to meet such application [1]. As compared to LEDs, vertical-cavity surface-emitting lasers (VCSELs) [2] at 850 nm wavelength naturally have more collimated output light beam, which can greatly save the cost of optics setup for long range light sensing and detection, such as the case of airborne light detecting and ranging (LIDAR) systems [3]. Furthermore, 850 nm VCSELs have attracted much attention due to their several unique advantages, such as, two-dimensional (2-D) array formation [4], [5], inexpensive device fabrication and characterization.

High-output-power and a single-lobe (spot) output with a low divergence angle and circular symmetry far-field pattern of VCSEL are thus highly desired for the above-mentioned applications. Increasing the effective diameter of the circular light-emitting aperture of a VCSEL is necessary to achieve a high output power. Extremely high output power (up to several watt's level) by paralleling a few hundred to a few 10,000's multi-mode VCSELs with advanced thermal package has been successfully demonstrated [6]. However, due to the multi-mode characteristic of each VCSEL unit, the divergence angle of combined far-field pattern is as wide as ∼20 degree. In addition, the peak of combined 2-D far-field pattern is usually very spotty instead of a Gaussian like smooth profile [6]. Several methods have been developed for VCSELs with single-mode and single-lobe output, such as the surface relief structure [7], Zn-diffusion structure [8], the 2-D holey structure (photonic crystal) [9], [10], anti-resonant reflecting optical waveguide structure [11], [12], and the combined application of implant and oxide apertures [13]. However, the maximum single-mode output power of these reported VCSELs is usually low (<7 mW) with a divergence angle at around 8 to 10^0 [7]–[13].

In order to further improve the performance in terms of power, beam shape, and divergence angle of a single-mode VCSEL unit, the photonic crystal (PC) based surface-emitting laser (array) structures has been demonstrated [14]. Such laser (array) can achieve large area coherent lasing with excellent single-mode output power (∼100 mW) and extremely narrow divergence angle ($\sim 2^0$) of circular symmetry far-field pattern [14] under continuous wave (CW) operation. Nevertheless, mass production of such device with complex 3-D nano-scale PC structure inside remains a challenge. In this paper, by use of Zn-diffusion technique for optical mode control, we demonstrate a 2-D single-mode VCSEL array structure with excellent lasing performance. A stable (invariable) single-lobe/near circular far-field pattern with a narrow full-width

Manuscript received April 1, 2014; revised June 24, 2014 and July 30, 2014; accepted August 1, 2014. Date of publication August 6, 2014; date of current version August 25, 2014. This work was supported in part by the Asian Office of Aerospace Research and Development under Grant AOARD-13-4086 and in part by the National Science Council of Taiwan under Grant NSC-101-2221-E-007-103-MY3 and Grant NSC-102-2622-E-009-012-CC1.

J.-L. Yen is with the Department of Information Technology, Takming University of Science and Technology, Taipei 114, Taiwan (e-mail: jlyen@takming.edu.tw).

K.-L. Chi, J.-W. Jiang, and J.-W. Shi are with the Department of Electrical Engineering, National Central University, Taoyuan 320, Taiwan (e-mail: porpoise5233@msn.com; ktkvsetko@gmail.com; jwshi@ee.ncu.edu.tw).

Y.-J. Yang is with the Department of Electrical Engineering, National Taiwan University, Taipei 106, Taiwan (e-mail: yjyang@cc.ee.ntu.edu.tw).

Color versions of one or more of the figures in this paper are available online at http://ieeexplore.ieee.org.

Digital Object Identifier 10.1109/JQE.2014.2345668

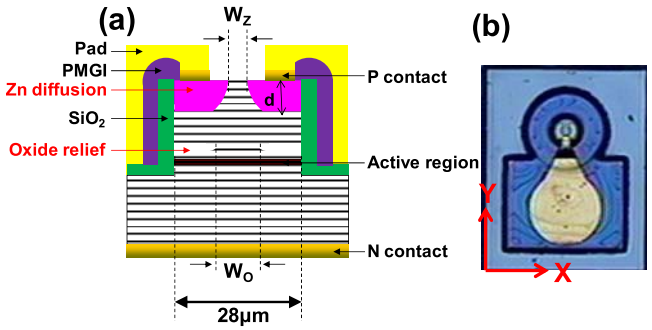

Fig. 1. (a) A conceptual cross-sectional view of unit VCSEL (W_Z/W_O/d: 6.5/9.5/1.5 μm), (b) top-view of unit VCSEL. x- and y- axes are used for defining the directions of 1-D far-field pattern measurements and simulations.

half maximum (FWHM) divergence angle ($\sim 4^0$) under the full range of bias current and a high maximum single-lobe output power (187.4 mW) under CW operation can be achieved. As compared to our previous work [15], significant improvement in output power (187.4 vs. 104 mW) with a narrower divergence (4^0 vs. 7.6^0) has been achieved. Such superior performance can be attributed to that the aperture (oxide and Zn-diffusion) sizes and the spacing between each single unit of VCSEL in the array have all been further optimized. These results also indicate that the high uniformity in our single-mode performance and weak in-phase (coherent) coupling between each VCSEL unit in our proposed device structure. A simple model has also been proposed to fit the measured far-field patterns and estimate the coherence in our array.

II. Device Structure and Measurement Results

Figure 1(a) and (b) show the conceptual cross-sectional and top views of the demonstrated unit VCSEL, respectively. As shown in Figure 1(a), there are three key parameters; W_Z, W_O, and d, which determines the mode characteristics of device. Here, W_Z and W_O represent the diameter of Zn-diffusion aperture and oxide-confined aperture, respectively. d is the Zn-diffusion depth. In order to attain stable single-mode performance under the whole range of bias current of each unit VCSEL, the relative sizes of these three parameters must be carefully optimized [15], [16]. First, the sizes of W_z and d must be usually less than around 6 and deeper than 1 μm, respectively [8], [16]. This empirical criterion is valid due to that we need a significant Zn-diffusion induced loss in the peripheral region of a small optical aperture to suppress the higher order mode. Lasing is suppressed in the Zn-diffused DBR region due to free-carrier absorption and reflectivity reduction caused by disordering [8]. Secondly, we must let $W_O > W_Z$ in our single-mode structure to ensure that there is a significant Zn-diffusion induced internal loss (α_i) in our current-confined (gain) region. According to our measurement results, such condition is the key to ensure the high uniformity in single-mode lasing performance of each unit VCSEL of array [16]. Here, we chose the values of W_o, W_z, and d, is around 9.5, 6.5, and 1.5 μm, respectively. Compared with the structure reported in our previous work [15], the sizes of W_o (9.5 vs. 8 μm) and W_z (6.5 vs. 5 μm) have both been enlarged in order to further narrow down the far-field divergence angle, increase the volume of optical cavity, and maximize the single-mode output optical power. A further increase in the diameter of Zn-diffusion aperture would result in output power enhancement but may induce a lot of higher order modes inside cavity.

The epi-layer structure, purchased from IQE[1] (IEGENS-7-20), is composed of three GaAs/$Al_{0.3}Ga_{0.7}As$ multiple-quantum-wells (MQWs) sandwiched between a 30-pair n-type and a 20-pair p-type $Al_{0.9}Ga_{0.1}As$/ $Al_{0.12}Ga_{0.88}As$ Distributed-Bragg-Reflector (DBR) layers with an $Al_{0.98}Ga_{0.02}As$ layer (30nm thickness) just above the MQWs for oxidation. The fabrication of array is started from the Zn-diffusion process. A high-quality Si_3N_4 film is necessary to serve as the mask for the high-temperature diffusion process. The mask defined diameter of the optical aperture (without Zn-diffusion) is around 8 μm. By considering the lateral Zn-diffusion, the final W_z is around 6.5 μm after the finish of Zn-diffusion process with a $\sim$1.5 μm depth (d). After that, the mesa etching process is performed. An oxidation technique is then used to define a circular current-confined area 9.5 μm in diameter. Under high-power and high-current density operations, the reliability of oxide-confined VCSEL is usually an issue [17]. In order to overcome such problem in our array, the AlO_x current-confined layer, has been removed by use of selective chemical wet etching (oxide-relief). Due to the excellent etching selectivity, such oxide-relief process would not at all degrade the performance of VCSEL [16]. In addition, the improvement in reliability of our structure can also be expected because of the elimination of oxide layer induced stress onto the neighboring active layers [17]. After p-type contact metallization (Ti/Au; 50/200 nm), the device is passivated by a SiO_2 layer ($\sim$150 nm) and a thick ($\sim$1.5 μm) polymethylglutarimide (PMGI) layer is then deposited for planarization. Finally, a thick Ti/Au ($\sim$1 μm) layer is evaporated onto chip to parallel different VCSEL units in the array and for on-wafer probing. As shown in Figure 1(a), the fabricated device has a 28 μm diameter active mesa and the n-type contact is realized in the bottom side of n-type GaAs substrate to uniform the current distribution especially in the array structure.

Figure 2(a) and (b) shows the measured light output power (L-I) and optical spectra under different bias current of a single VCSEL unit, respectively. The uniformity of single-mode performance between different VCSEL units is very high. Here, the measured L-I curves of three devices on the same chip are shown in Figure 2(a) for reference. As can be seen, the single device exhibits a threshold current at 1.7 mA and can sustain highly single-mode operation (side-mode suppression ratio (SMSR) $>$30 dB) under the full range of bias current (from threshold to saturation) with a maximum single-mode power up to 7.1 mW.

Such value is as high as the record of maximum single-mode output power ($\sim$7 mW) of 850 nm VCSELs [7], [8]. Figure 3 shows the measured one-dimensional (1-D) (in the x-direction) and 2-D far-field patterns of single device under different bias currents. Regarding with the 1-D far-field pattern measurement, it is realized by use of a rotational arm, which is

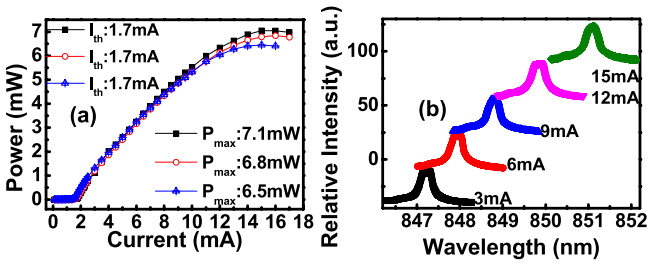

Fig. 2. The measured (a) L-I curves and (b) optical spectra under different bias currents of unit VCSEL.

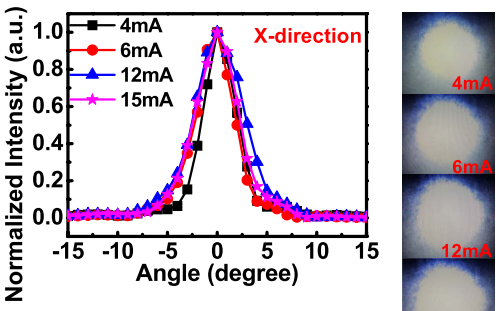

	4mA	6mA	12mA	15mA
X	3.8°	4.3°	5.8°	4.9°
Y	5.7°	5.4°	7.2°	5.1°

Fig. 3. The measured 1-D (in x-direction) and 2-D far-field patterns under different bias currents of unit VCSEL. The inserted Table shows the FWHM of measured divergence angles under different bias currents in both directions.

connected with a well-calibrated optical sensor head with a slit mounted on its window. The distance between sensor head and device under test is around 13 cm. During our measurement, the width of slit is set as less than 1 mm. With a 13 cm distance between slit and device under test, the resolution for divergence angle measurement should be around 0.44 degree. Such resolution is high enough to accurately measure the divergence angles with the values what we will claim latter (∼5 degree) in this paper. For the case of 2-D measurement, a charge-coupled device (CCD) camera is installed just above the array for making pictures of its far-field pattern. In order to avoid the saturation of camera and influence of optical feedback effect on the measured patterns, neutral density (ND) filters with a tilted angle are inserted between array and CCD.

The inserted Table in Figure 3 shows the measured FWHM of divergence angles in both x- and y- directions under different bias currents. Such two directions are specified on the top-view of fabricated device, as shown in Figure 1 (b). The values of divergence angles shown in this paper are all measured by using the setup of rotational arm. We can clearly see that due to its excellent single-mode characteristics as discussed in Figure 2, a far-field pattern with narrow divergence angle (4^0∼5^0) in both directions can be achieved. By use of the far-field assumptions of Gaussian optics reported in Ref. [18] and [19], our measured 1-D far-field distribution, as shown in Figure 3, can be fitted by the following equation 1:

$$I(r) \approx I_0 \exp\left(-2r^2/w_0^2\left[1+\left(\frac{\lambda z}{\pi w0}\right)^2\right]\right) \qquad (1)$$

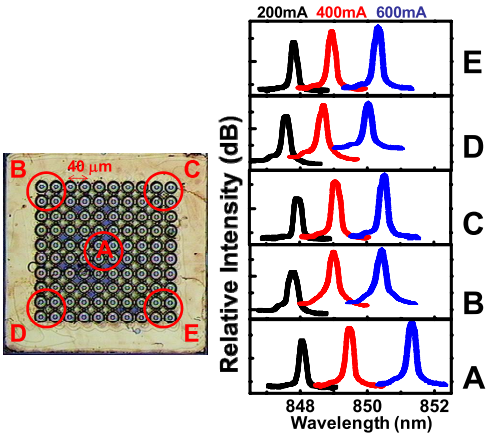

Fig. 4. The measured bias dependent output optical spectra in different portions of 10 × 10 array with a 40 μm spacing between neighbor units.

Where, $I(r)$ is the intensity distribution function of the far-field pattern, I_0 is a constant, λ is wavelength (0.85 μm), z is the distance between light source and measurement point, and w_0 is the minimum beam radius. By using the extracted values of w_0, we can then determine the M^2 factor, which is an important parameter to evaluate the laser beam quality [19], [20]. Here, z equals to 13 cm in our measurement setup, which is much larger than the extracted values of w_0 (as discussed latter). This indicates the validness of our far-filed assumption.

Under a 6 mA bias current, the extracted w_0 of single-unit VCSEL in x- and y- directions is 4.3 and 3.4 μm, respectively. These values are close to the size of Zn-diffusion apertures. All the extracted values of w_0 in different array structure are given in Table II. The different values of w_0 in x- and y- directions imply an elliptical near-field pattern in our VCSEL. Such discrepancy between ideal circular Zn-diffusion apertures (∼3.3 μm in radius) is mainly due to the unintentional misalignment between Zn-diffusion and oxide apertures. We can clearly understand if two circles don't perfectly concentric alignment, their outline should look like elliptical shape. This phenomenon explains that we why we usually get larger values of divergence angles in one axis than that of measured in other axis. The non-perfect alignment between gain (oxide-aperture) and loss (Zn-diffusion) regions in our single-mode VCSEL may also be used to explain the randomly variation (broadening) of measured divergence angle with the increase of bias currents (4 to 15 mA). With the extracted values of w_0, we can roughly estimate values of M^2 factor, which is around ∼1.2 in both x- and y-directions. Such number represents that our single-mode VCSEL output beam is nearly diffraction limited ($M^2 \approx 1$) [19], [20].

Figure 4 and 5 shows the top-view of fabricated 10 × 10 array with different spacing between neighbor unit as 40 and 66 μm (as specified on the Figures), respectively. As can be seen, we simply parallel each unit VCSEL by connecting their p-type metals with a large metal pad for probing or wire bonding. All the unit devices are common ground through the use of bottom n-type contact layer on the n-type GaAs substrate.

Here, two different spacing between units (40 and 66 μm) are chosen to fabricate our arrays. The 40 μm spacing is the minimum size we can fabricate for the 28 μm mesa diameter.

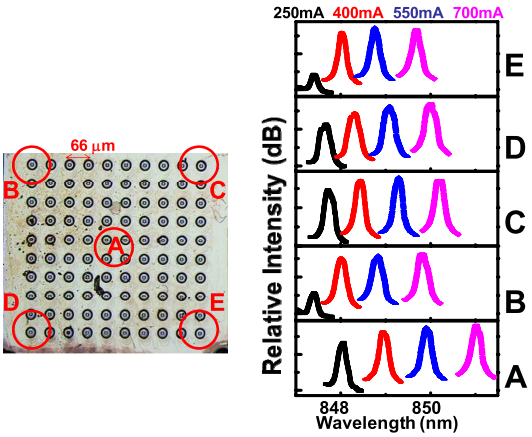

Fig. 5. The measured bias dependent output optical spectra in different portions of 10 × 10 array with a 66 μm spacing between neighbor units.

To further down scale the mesa diameter and spacing between VCSEL units would increase the difficulty in p-type contact metallization and planarization processes, respectively. On the other hand, by increasing the spacing to 66 μm, we may expect that there is an improvement in device heat-sinking under high-power operation. The detail comparison of L-I performances between 66 and 40 μm spacing array will be discussed latter.

In contrast to most of the reported semiconductor laser array [4], [5], where each light-emission aperture shares the same optical cavity and its optical near-field usually has strong overlap (coupling), in our proposed array structure the optical near field of each single-mode unit (aperture) is isolated by different mesa with a significant spacing. The strong phase locking (coherent lasing) between different emitters and significant narrowing of array's far-field divergence angle thus cannot be expected in our structure. Nevertheless, if each unit in our proposed array structure has very similar single-mode performance, we still can expect that the divergence angle of array can be as narrow as that of a single-mode unit VCSEL and the total output power can be as high as the summation of power from all the VCSEL units. The detail working principal of our proposed array structure will be discussed in the next section about device modeling.

Figure 6 (a) and (b) shows the measured L-I curves of 6 × 6 and array 10 × 10 with different spacing (66 and 40 μm) between single units, respectively. Although we may expect that the larger unit spacing can benefit the heat dissipation of array under high power operation, the L-I performance of 40 μm spacing array is really superior to that of 66 μm spacing for both the cases of 6 × 6 and 10 × 10 array, as shown in Figure 6(a) and (b). The similar trend of result is repeatable in different arrays across the whole chip. Here, two sets (four traces) of measured L-I curves of 6 × 6 array are given in Figure 6(a) for references. The better performance of 40 μm spacing array might be attributed to its smaller chip size and more uniform device performance of single unit VCSEL in the array as compared to that of 66 μm spacing structure. The non-uniform characteristic of single unit in the array is mainly originated from misalignment between oxide and Zn-diffusion apertures and the non-perfect uniformity of VCSEL wafer itself. Both of them would become more

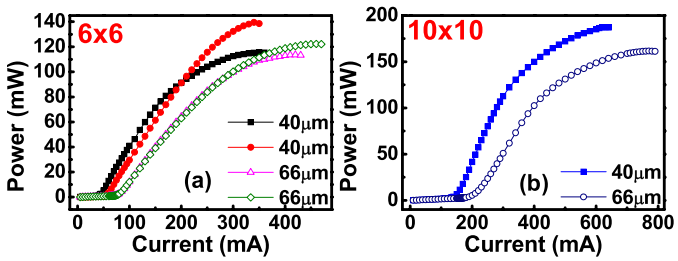

Fig. 6. The measured L-I curves of (a) 6 × 6 and (b) 10 × 10 array with a 40 and 66 μm spacing between neighboring unit.

significant when the chip area is increased. This is supported by the measurement results of single-unit reference VCSELs, which were fabricated along the edges of our array. Compared with 66 μm spacing array with a larger chip size, the difference in L-I performance of reference unit VCSELs along four edges of 40 μm spacing array is usually less pronounced. The other possible reason for superior performance of array with 40 μm spacing to that of 66 μm spacing one is its smaller lateral resistance. A less device heating and better high-power performance of 40 μm spacing array can thus be observed. The measured differential resistances of 10 × 10 array with a 40 and 66 μm unit spacing under a 500 mA forward bias current is around 2.5∼4 Ω and 8.5∼10 Ω, respectively. During array measurement, we always probe on one of its edges and the injected current would thus laterally spread out the whole chip and terminate at the bottom side n-contact on the n+ GaAs substrate. The higher differential resistance of 66 μm spacing device can thus be attributed to its larger lateral distance for current spreading.

The maximum output power of 6 × 6 and 10 × 10 array (40 μm spacing) is as high as 140 and 187.4 mW, respectively. Compared with the maximum output power reported in our previous work [15], the significant improvement (140 vs. 104 mW) in power performance for the same size of array (6 × 6) is due to that we adopt a larger diameters of oxide and Zn-diffusion apertures (W_o: 9.5 vs. 8 μm; W_z: 6.5 vs. 5 μm), which would lead to a larger size of optical cavity, smaller differential resistance, and better device heat-sink under high-power operation. Furthermore, we can clearly see that although the number of VCSEL units greatly increase from 36 to 100, the improvement in maximum output power is marginal (140 to 187.4 mW). This implies that the device heating seriously limits the maximum output power of our array structure [15]. An improved package, which considers thermal effect, is definitely necessary to further increase the number of VCSEL units in our proposed array structure and its maximum output power [6]. Figures 4 and 5 shows the measured bias dependent output optical spectra of 6 × 6 and 10 × 10 array (at different portions of array), respectively. As can be seen, although the phase-locking between each unit VCSEL in the array is small, which will be discussed in next section, the measured spectra in different portion of array is highly single-mode (SMSR >30 dB) and very similar. This indicates that the uniformity of single-mode performance of each VCSEL unit in our array is high. In addition, a less device-heating phenomenon of 40 μm spacing array is also supported by the measured optical spectra. Figure 7 shows the

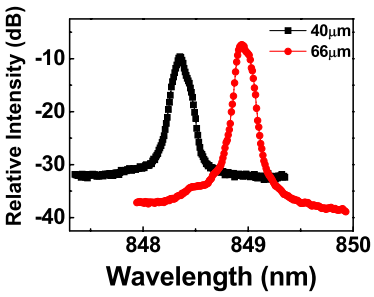

Fig. 7. The measured output optical spectra in position A of 10 × 10 array with 40 and 66 μm spacing and under the same output optical power (100 mW).

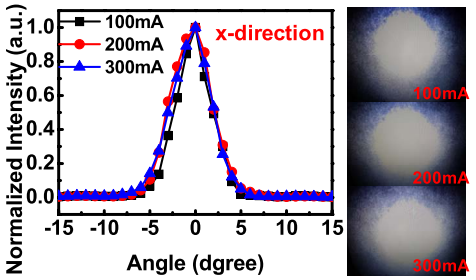

	100mA	200mA	300mA
X	3.2°	4.3°	5.6°
Y	4.4°	5.2°	5.1°

6X6
Space:40μm

Fig. 8. The measured 1-D (x-direction) and 2-D far-field patterns under different bias currents of 10 × 10 array with 40 μm spacing between neighbor units. The inserted Table shows the FWHM of measured divergence angles under different bias currents in both directions.

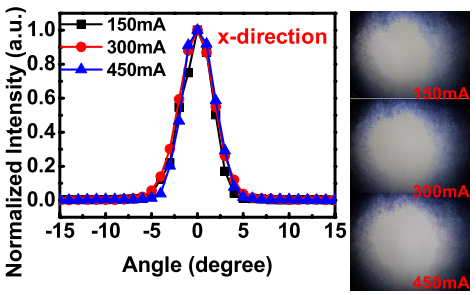

	150mA	300mA	450mA
X	4.5°	4°	3.5°
Y	4.1°	4.4°	4.2°

6X6
Space:66μm

Fig. 9. The measured 1-D (x-direction) and 2-D far-field patterns under different bias currents of 6 × 6 array with 66 μm spacing between neighbor units. The inserted Table shows the FWHM of measured divergence angles under different bias currents in both directions.

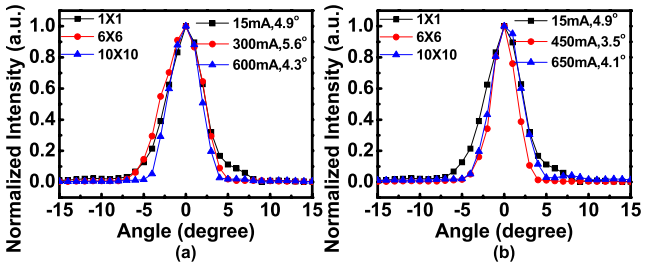

Fig. 10. The measured 1-D (x-direction) far-field patterns of single device 6 × 6, and 10 × 10 array under 15, 300, and 600 mA bias currents, respectively, with (a) 40 and (b) 66 μm spacing between neighbor unit.

measured optical spectra of 10 × 10 array with 40 and 66 μm spacing at "position A", as specified in Figure 4 and 5. Both devices are measured under the same output optical power (∼100 mW) and have the same starting central wavelengths at 848 nm when the bias current is just above threshold. The longer central wavelength of 66 μm spacing array than that of 40 μm one indicates the higher junction temperature in 66 μm one.

Figure 8 and 9 shows the measured 1-D and 2-D far-field patterns under different bias current of 6 × 6 array with 40 and 66 μm spacing, respectively. Take the structure with 66 μm spacing for example, if a perfectly (100 %) phase-locking phenomenon happens in this structure with such a large area (330 × 330 μm^2), the theoretical diffraction-limited divergence angle should be as small as around 0.1^0. However, this value doesn't match which we have measured ($4\sim5^0$).

Figure 10(a) and (b) shows the detail comparison of 1-D far-field patterns of single-element VCSEL, 6 × 6, and 10 × 10 array with 40 and 66 μm spacing between neighbor units, respectively. As can be seen, the measured far-field divergence angles of 6 × 6 or 10 × 10 arrays are very similar with that of single reference device ($\sim4^0$ vs. $\sim5^0$). We may thus conclude that the in-phase-locking effect in our array is weak and the detail would be discussed in the following section.

The in-phase (coherent) lasing phenomenon is highly desired in the semiconductor laser array structure due to it can greatly narrow down the far-field divergence angle. However, the fundamental mode of array structure is usually out-of-phase (180^0 phase difference) lasing mode, which would induce donut-shape far-field patterns [4], [5], [21]. In addition, the far-field pattern of phase-locking array usually varies seriously with the increase in bias current [4], [5], [21] and accompanies with lots of side-lobes. On the other hand, although in our proposed array structure the phase locking phenomenon is weak as discussed, the uniformity of single-mode characteristic of each lasing unit is very high. This would lead to that the far-field pattern and divergence angle of free-space combined optical beams of array is as good as that of our single VCSEL unit, as discussed in Figure 3. Furthermore, a strong enhancement in total output power, which is proportional to the number of VCSEL units in the array, can also be obtained due to free-space optical power combining.

Among all the discussed device structures in this paper, the demonstrated array with 40 μm device spacing has the best performance in terms of power and divergence angle. Figure 11 shows its 1-D (x-direction) and 2-D far-field patterns under different bias currents. As can be seen, even under saturation bias current (600 mA), our device can sustain a $\sim4^0$ divergence angle with extremely high output power (187.4 mW). Furthermore, its single-spot and narrow far-field distribution can be sustained from near threshold till saturation. Table I shows the benchmark of high-performance single-mode surface-emitting laser (SEL) array at

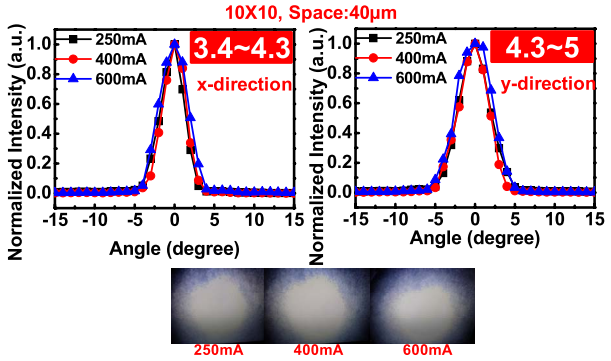

Fig. 11. The measured 1-D (in x- and y- directions) and 2-D far-field patterns under different bias currents of array with 40 μm spacing between neighboring units. The FWHM of divergence angle is specified.

TABLE I
COMPARSION OF FIGURE OF MERIT FOR STATE-OF-THE-ART SINGLE-MODE SEL ARRAY

	Kyoto University[22]	UWM[12]	UIUC[10]	NCU previous Work[15]	NCU this work
Efficiency(%)	~31	~3	~20	~41	~41
Divergence angle	<2°	1.61°	3°	4.2~7.6°	3~4°
Output power(Max)	60mW	<10mW	1.4mW	104mW	187.4mW
Operation Mode	CW	Pulse	CW	CW	CW

850 [10], [12], [15] and 960 nm [14], [22] wavelengths. We can clearly see that our demonstrated structure can achieve excellent slope efficiency with very-high output optical power and sustain a narrow far-field divergence angle among the reported single-mode SEL array structures.

III. SIMULATION AND MODELING RESULTS

As shown in Figure 10, compared with single-device, the measured divergence angle of array still shows slightly narrowing and this reflects that the "non-zero" coherence exists in our array structure. In order to roughly estimate the value of weak coherence in our array, in this section, we propose a model to fit and explain the measured far-field patterns of single VCSEL and VCSEL array. According to the fitting and modeling results, we can then determine the coupling coefficient between each unit light emitter in our array. Figure 12(a) and (b) shows the conceptual diagram of our mathematical model used for single element and array's far-field patterns calculation, respectively.

As shown in Figure 12(a), we divide our light-emitting aperture (with a ~6.5 μm diameter) into several meshes (40 × 40 pixels) and the far-field pattern contributed by each pixel can be expressed by equation 2 as follows:

$$I(r) \propto \left(\iint_{\text{aperture}} e^{-\frac{(r')^2}{2\sigma^2}} e^{-jk(r-r')} dx' dy' \right)^2 \quad (2)$$

Here, we adopt the plane wave assumption (Fraunhofer diffraction formula [23]) with a Gaussian (normal) distribution in our

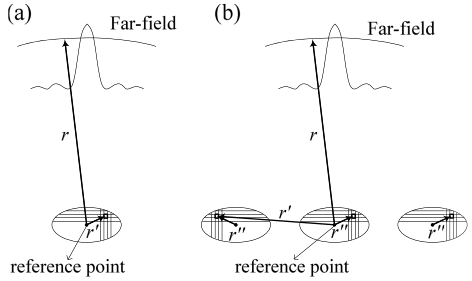

Fig. 12. The conceptual diagram for far-field pattern calculations of (a) single VCSEL and (b) VCSEL array.

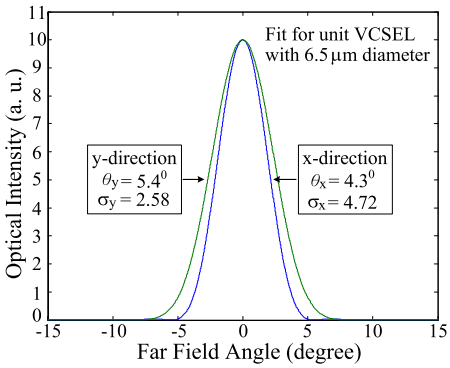

Fig. 13. The simulated far-field pattern in x- and y- axis of single VCSEL under 6 mA bias current.

far-field pattern [18]. Where, $I(r)$ is the intensity distribution function of the far-field pattern, σ is the standard deviation of Gaussian far-field distribution, and k is the wave number. The definitions of r and r' are specified on Figure 12(a). By use of such established model, we can then fit the measured far-field pattern of our single device as discussed in Figure 3. Figure 13 shows the simulated far-field patterns in x- and y- directions. In order to get good fitting results with the measured divergence angle under 6 mA bias current, the values of σ in x- (σ_x) and y- (σ_y) directions must be chosen carefully. Their values are specified on the Figure.

Regarding with the calculation of array's far-field pattern, it can be realized by use of equation 3 [18], [23] as follows:

$$I(r) \propto \left(\iint_{\text{aperture}} e^{-\frac{(r'')^2}{2\sigma^2}} e^{-jk(r-r')} dx' dy' \right)^2 \quad (3)$$

The only difference between equation 2 and 3 is only in the variable r'' in the Gaussian distribution function. As shown in Figure 12 (b), for the case of array, r' and r'' represents the spatial variable between different light-emitting aperture (LEA) and inside a single LEA, respectively. During simulation of array, the extracted values of σ_x and σ_y of single VCSEL, as discussed in Figure 13, have been adopted for calculation. In addition, in equation 3, any random variation of phase (non-coherence) between different LEAs is not considered. It means that the coherence in this array is 100% and Figure 14 shows the simulated results. We can clearly see that due to the above assumption (perfect coherence), the FWHM of main lobe's divergence angle in the simulated far-field pattern is as narrow as 0.17^0 for the case of

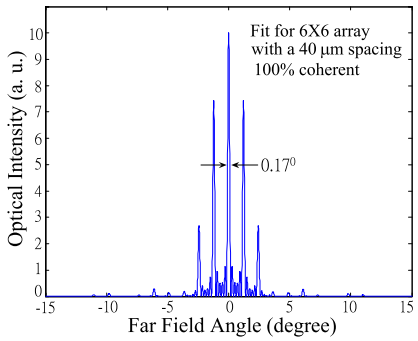

Fig. 14. The simulated far-field pattern in x- and y- axis of array (40 μm spacing) with 100% coherence.

TABLE II
EXTRACTED VALUES OF STANDARD DEVIATION (σ), MINIMUM BEAM RADIUS (W_0), AND COUPLING COEFFICIENT (γ) OF SINGLE VCSEL AND VCSEL ARRAY (SAPCING: 40 μm) AT x- AND y- AXES

Size	Direction	Injected Current	Measured Angle	σ (μm)	W_0 (μm)	γ (%)
1x1	x	6mA	4.3º	4.7	4.3	--
6x6	x	200mA	4.3º	4.7	4.3	8×10^{-5}
10x10	x	400mA	3.3º	10.4	5.6	4.6
1x1	y	6mA	5.4º	2.6	3.4	--
6x6	y	200mA	5.2º	2.8	3.5	0.13
10x10	y	400mA	4.3º	4.7	4.3	1.7

6 × 6 array (40 μm spacing). Such simulated result apparently doesn't match with the measurement results as shown in Figures 8 to 11 and indicate the weak coherence in our array.

In order to estimate the value of coherence in our array, the following approach has been adopted. First, by use of equation 2 and the simulated main lobe in the far-field pattern of array, as shown in Figure 14, we can extract the values of σ_x and σ_y. These two values are the key parameters which determine the far-field pattern of 100 % coherent array. On the other hand, the values of σ_x and σ_y of single unit VCSEL, as discussed in Figure 13, is just the case of 0 % coherence in the array. According to our measured far-field pattern of array, we can further extract its corresponding values of σ_x and σ_y. Based on this value and the values of σ_x and σ_y in two extreme cases of coherence (0 and 100%), we can finally determine the coherence in our array on both axes (x- and y-axes) through the use of linear interpolation. Table II shows the extracted values of coherence (γ), near-field minimum beam radius (w_0), and far-field σ of single device and arrays (40 μm spacing) at both x- and y- axes under different bias currents. As can be seen, the coherence in our array structure is very low as discussed. Nevertheless, the far-field pattern of our array is close with that of single-mode unit VCSEL, which has a near diffraction-limited beam quality ($M^2 \approx 1.2$), as discussed in Figure 3.

IV. CONCLUSION

In conclusion, we demonstrate a novel single-mode VCSEL array structure. By properly controlling the sizes of Zn-diffusion and oxide apertures, each unit VCSEL in the whole array has highly uniform single-mode performance. An excellent lasing phenomenon has been observed in our 10 × 10 array, and it exhibits a stable single-lobe/near circular far-field pattern with a narrow FWHM divergence angle ($\sim 4^0$) under the full range of bias current and a high maximum single-lobe output power (187.4 mW) under CW operation. The far-field pattern simulation result indicates that although the coherence in our array is low, the output beam quality is as good as a single-mode unit VCSEL with the near-diffraction limited output optical beam (M^2 10 × 10).

REFERENCES

[1] R. Stevenson, "Epistar unveils efficient infrared LED," *Compound Semicond.*, vol. 20, p. 7, Jan./Feb. 2014.
[2] F. Koyama, S. Kinoshita, and K. Iga, "Room-temperature continuous wave lasing characteristics of a GaAs vertical cavity surface-emitting laser," *Appl. Phys. Lett.*, vol. 55, pp. 221–222, Jul. 1989.
[3] J. A. Reagan, H. Liu, and J. F. McCalmont, "Laser diode based new generation lidars," in *Proc. Symp. IGARSS*, May 1996, pp. 1535–1537.
[4] M. E. Warren *et al.*, "On-axis far-field emission from two-dimensional phase-locked vertical cavity surface-emitting laser arrays with an integrated phase-corrector," *Appl. Phys. Lett.*, vol. 61, no. 13, pp. 1484–1486, Sep. 1992.
[5] M. Orenstein, E. Kapon, J. P. Harbison, L. T. Florez, and N. G. Stoffel, "Large two-dimensional arrays of phase-locked vertical cavity surface emitting lasers," *Appl. Phys. Lett.*, vol. 60, pp. 1535–1537, Mar. 1992.
[6] J.-F. Seurin *et al.*, "Efficient vertical-cavity surface-emitting lasers for infrared illumination applications," *Proc. SPIE, Vertical-Cavity Surface-Emitting Lasers XV*, vol. 7952, p. 79520G, Feb. 2011.
[7] Å. Haglund, J. S. Gustavsson, J. Vukusić, P. Modh, and A. Larsson, "Single fundamental-mode output power exceeding 6 mW from VCSELs with a shallow surface relief," *IEEE Photon. Technol. Lett.*, vol. 16, no. 2, pp. 368–370, Feb. 2004.
[8] J.-W. Shi, C.-C. Chen, Y.-S. Wu, S.-H. Guol, and Y.-J. Yang, "High-power and high-speed Zn-diffusion single fundamental-mode vertical-cavity surface-emitting lasers at 850-nm wavelength," *IEEE Photon. Technol. Lett.*, vol. 20, no. 13, pp. 1121–1123, Jul. 1, 2008.
[9] A. Furukawa, S. Sasaki, M. Hoshi, A. Matsuzono, K. Moritoh, and T. Baba, "High-power single-mode vertical-cavity surface-emitting lasers with triangular holey structure," *Appl. Phys. Lett.*, vol. 85, pp. 5161–5163, Nov. 2004.
[10] D. F. Siriani and K. D. Choquette, "Electronically controlled two-dimensional steering of in-phase coherently coupled vertical-cavity laser arrays," *IEEE Photon. Technol. Lett.*, vol. 23, no. 3, pp. 167–169, Feb. 1, 2011.
[11] D. Zhou and L. J. Mawst, "High-power single-mode antiresonant reflecting optical waveguide-type vertical-cavity surface-emitting lasers," *IEEE J. Quantum Electron.*, vol. 38, no. 12, pp. 1599–1606, Dec. 2002.
[12] L. Bao *et al.*, "Near-diffraction-limited coherent emission from large aperture antiguided vertical-cavity surface-emitting laser arrays," *Appl. Phys. Lett.*, vol. 84, pp. 320–322, Jan. 2004.
[13] E. W. Young, K. D. Choquette, S. L. Chuang, K. M. Geib, A. J. Fischer, and A. A. Allerman, "Single-transverse-mode vertical-cavity lasers under continuous and pulsed operation," *IEEE Photon. Technol. Lett.*, vol. 13, no. 9, pp. 927–929, Sep. 2001.
[14] S. Noda, "Photonic crystal lasers—Ultimate nanolasers and broad-area coherent lasers [Invited]," *J. Opt. Soc. Amer. B*, vol. 27, pp. B1–B8, Nov. 2010.
[15] J.-W. Shi, K.-L. Chi, J.-H. Chang, Z.-R. Wei, J.-W. Jiang, and Y.-J. Yang, "Single-mode vertical-cavity surface-emitting laser array with high power and narrow far-field divergence angle," *IEEE Photon. J.*, vol. 5, no. 6, Dec. 2013, Art. ID 1502508.
[16] J.-W. Shi *et al.*, "Single-mode, high-speed, and high-power vertical-cavity surface-emitting lasers at 850 nm for short to medium reach (2 km) optical interconnects," *J. Lightw. Technol.*, vol. 31, no. 24, pp. 4037–4044, Dec. 15, 2013.
[17] R. W. Herrick, A. Dafinca, P. Farthouat, A. A. Grillo, S. J. McMahon, and A. R. Weidberg, "Corrosion-based failure of oxide-aperture VCSELs," *IEEE J. Quantum Electron.*, vol. 49, no. 12, pp. 1045–1052, Dec. 2013.

[18] R. S. Quimby, "Gaussian beam optics," in *Photonics and Lasers: An Introduction*. Hoboken, NJ, USA: Wiley, 2006, ch. 17, pp. 307–309.
[19] A. E. Siegman, "Physical properties of Gaussian beams," in *Lasers*, Sausalito, CA, USA: Univ. Science Books, 1986, ch. 17, pp. 663–695.
[20] A. E. Siegman, "Defining, measuring, and optimizing laser beam quality," *Proc. SPIE, Laser Resonators Coherent Opt., Model., Technol., Appl.*, vol. 1868, p. 2, Jan. 1993.
[21] J.-W. Shi, J.-L. Yen, C.-H. Jiang, K.-M. Chen, T.-J. Hung, and Y.-J. Yang, "Vertical-cavity surface-emitting lasers (VCSELs) with high-power and single-spot far-field distributions at 850-nm wavelength by use of petal-shaped light-emitting apertures," *IEEE Photon. Technol. Lett.*, vol. 18, no. 3, pp. 481–483, Feb. 1, 2006.
[22] K. Otsuka *et al.*, "High-power surface-emitting photonic crystal laser," in *Proc. IEEE Annu. Meeting Lasers Electro-Opt. Soc. (LEOS)*, Orlando, FL, USA, Oct. 2007, no. WR-2, pp. 562–563.
[23] R. D. Guenther, "Diffraction," in *Modern Optics*, 1st ed. New York, NY, USA: Wiley, 1990, ch. 7, pp. 106–120.

Jia-Liang Yen was born in Kaohsiung, Taiwan, in 1969. He received the M.S. degree and the Ph.D. degree in electrical engineering from National Taiwan University, Taipei, Taiwan, in 1998 and 2004, respectively. He is currently an Assistant Professor with the Department of Information Technology, Takming University of Science and Technology, Taipei. His research interests include cloud computing and artificial intelligence, in particular, power control of cloud system.

Kai-Lun Chi was born in New Taipei, Taiwan, in 1988. He is currently pursuing the Ph.D. degree with the Department of Electrical Engineering, National Central University, Taoyuan, Taiwan. His current research interests include high-speed optoelectronic device measurement, and high-speed VCSELs and LEDs for the application of optical interconnects.

Jia-Wei Jiang was born in Taichung, Taiwan, in 1989. He is currently pursuing the master's degree with the Department of Electrical Engineering, National Central University, Taoyuan, Taiwan. His current research interests include mass production of high-speed and high-reliability VCSELs for the application of optical interconnects.

Ying-Jay Yang was born in Yilan, Taiwan, in 1952. He received the B.S. degree in electrical engineering from National Taiwan University, Taipei, Taiwan, in 1974, and the M.S. degree and the Ph.D. degree in electrical engineering from North Carolina State University, Raleigh, NC, USA, in 1982 and 1987, respectively. During the Ph.D. work, he invented the first quantum well transverse junction stripe (TJS) lasers and also the first CW operation strained-layer TJS lasers. From 1987 to 1989, he was an Engineer with Hewlett Packard, Palo Alto, CA, USA, working on the development of 1.3-μm InGaAsP LEDs for FDDI. From 1989 to 1993, he was with the Lockheed Palo Alto Research Laboratory, Palo Alto, as a Research Scientist. He worked on the vertical-cavity surface emitting lasers (SELs), and invented the first single transverse mode SELs and the first optoelectronic integration circuits (OEICs) with a SEL and FET. In 1993, he joined the Department of Electrical Engineer at National Taiwan University, where he is currently a Professor. His current research interests include semiconductor materials, and devices, including lasers, modulators, quantum devices, and OEICs.

Jin-Wei Shi was born in Kaohsiung, Taiwan, in 1976. He received the B.S. degree in electrical engineering from National Taiwan University, Taipei, Taiwan, in 1998, and the Ph.D. degree from the Graduate Institute of Electro-Optical Engineering, National Taiwan University, in 2002. He was a Visiting Scholar with the University of California at Santa Barbara (UCSB), Santa Barbara, CA, USA, from 2000 to 2001. From 2002 to 2003, he served as a Post-Doctoral Researcher with Electronic Research and Service Organization, Industrial Technology Research Institute, Hsinchu, Taiwan. In 2003, he joined the Department of Electrical Engineering, National Central University, Taoyuan, Taiwan, where he is currently a Professor. In 2011, he joined the Department of Electrical and Computer Engineering at UCSB as a Visiting Scholar. His current research interests include ultrahigh-speed/power optoelectronic devices, such as photodetectors, electroabsorption modulator, submillimeter-wave photonic transmitter, and semiconductor laser. He has authored and co-authored more than 100 SCI journal papers, 180 conference papers, and hold 25 patents. He was an invited speaker of the 2002 IEEE LEOS, the 2005 SPIE Optics East, the 2007 Asia-Pacific Microwave Photonic (MWP) conference, the 2008 Asia Optical Fiber Communication and Optoelectronic Exposition and Conference, the 2011 Optical Fiber Communication (OFC) conference, and the 2012 IEEE Photonic Conference. He served as a Technical Program Committee Member of 2009–2011 OFC, 2012 SSDM, 2012 MWP, 2013 Asia-Pacific CLEO, 2014 IPRM, and 2014 OECC. He was a recipient of the 2007 Excellence Young Researcher Award from the Association of Chinese IEEE and the 2010 Da-You Wu Memorial Award.